

JLab Measurements of the ^3He Form Factors at Large Momentum Transfers

A. Camsonne²², A.T. Katramatou¹¹, M. Olson²⁰, A. Acha⁴, K. Allada¹², B.D. Anderson¹¹, J. Arrington¹, A. Baldwin¹¹, J.-P. Chen²², S. Choi¹⁸, E. Chudakov²², E. Cisbani^{8,10}, B. Craver²³, P. Decowski¹⁹, C. Dutta¹², E. Folts²², S. Frullani^{8,10}, F. Garibaldi^{8,10}, R. Gilman^{16,22}, J. Gomez²², B. Hahn²⁴, J.-O. Hansen²², D. W. Higinbotham²², T. Holmstrom¹³, J. Huang¹⁴, M. Iodice⁹, X. Jiang¹⁶, A. Kelleher²⁴, E. Khrosinkova¹¹, A. Kievsky⁷, E. Kuchina¹⁶, G. Kumbartzki¹⁶, B. Lee¹⁸, J.J. LeRose²², R.A. Lindgren²³, G. Lott²², H. Lu¹⁷, L.E. Marcucci^{7,15}, D.J. Margaziotis², P. Markowitz⁴, S. Marrone⁶, D. Meekins²², Z.-E. Meziani²¹, R. Michaels²², B. Moffit¹⁴, B. Norum²³, G.G. Petratos¹¹, A. Puckett¹⁴, X. Qian³, O. Rondon²³, A. Saha²², B. Sawatzky²¹, J. Segal²², M. Shabestari²³, A. Shahinyan²⁵, P. Solvignon¹, N. Sparveris^{11,21}, R.R. Subedi²³, R. Suleiman²², V. Sulkosky²², G.M. Urciuoli⁸, M. Viviani⁷, Y. Wang⁵, B.B. Wojtsekhowski²², X. Yan¹⁸, H. Yao²¹, W.-M. Zhang¹¹, X. Zheng²³, and L. Zhu⁵

¹Argonne National Laboratory, Argonne, IL 60439, USA

²California State University, Los Angeles, CA 90032, USA

³Duke University (TUNL), Durham, NC 27708, USA

⁴Florida International University, Miami, FL 33199, USA

⁵University of Illinois at Urbana Champagne, Urbana, IL 61801, USA

⁶Istituto Nazionale di Fisica Nucleare, Sezione di Bari and University of Bari, 70126 Bari, Italy

⁷Istituto Nazionale di Fisica Nucleare, Sezione di Pisa, 56127 Pisa, Italy

⁸Istituto Nazionale di Fisica Nucleare, Sezione di Roma, 00185 Rome, Italy

⁹Istituto Nazionale di Fisica Nucleare, Sezione di Roma Tre, 00146 Rome, Italy

¹⁰Istituto Superiore di Sanità, 00161 Rome, Italy

¹¹Kent State University, Kent OH 44242, USA

¹²University of Kentucky, Lexington, KY 40506, USA

¹³Longwood University, Farmville, VA 23909, USA

¹⁴Massachusetts Institute of Technology, Cambridge, MA 02139, USA

¹⁵University of Pisa, 56127 Pisa, Italy

¹⁶Rutgers, The State University of New Jersey, Piscataway, NJ 08855, USA

¹⁷University of Science and Technology of China, Hefei, Anhui, 230026 P.R. China

¹⁸Seoul National University, Seoul 151-747, Korea

¹⁹Smith College, Northampton, MA 01063, USA

²⁰St. Norbert College, De Pere WI 54115, USA

²¹Temple University, Philadelphia, PA 19122, USA

²²Thomas Jefferson National Accelerator Facility, Newport News, VA 23606, USA

²³University of Virginia, Charlottesville, VA 22904, USA

²⁴College of William and Mary, Williamsburg, VA 23185, USA and

²⁵Yerevan Physics Institute, Yerevan 375036, Armenia

The charge and magnetic form factors, F_C and F_M , of ^3He have been extracted in the kinematic range $25 \text{ fm}^{-2} \leq Q^2 \leq 61 \text{ fm}^{-2}$ from elastic electron scattering by detecting ^3He recoil nuclei and electrons in coincidence with the High Resolution Spectrometers of the Hall A Facility at Jefferson Lab. The measurements are indicative of a second diffraction minimum for the magnetic form factor, which was predicted in the Q^2 range of this experiment, and of a continuing diffractive structure for the charge form factor. The data are in qualitative agreement with theoretical calculations based on realistic interactions and accurate methods to solve the three-body nuclear problem.

PACS numbers: 25.30.Bf, 13.40.Gp, 27.10.+h, 24.85.+p

Elastic electron scattering from nuclei has been a basic tool in the study of their size and associated charge and magnetization distributions [1]. It allows for the extraction of their electromagnetic (EM) form factors, which in the case of few-body nuclear systems can be compared with state-of-the-art theoretical calculations. The few-body form factors are considered the “observables of choice” [2] for testing the nucleon-meson standard model of the nuclear interaction and the associated EM current operator [3]. They provide fundamental information

on the internal structure and dynamics of light nuclei as they are, at the simplest level, convolutions of the nuclear ground state wave function with the EM form factors of the constituent nucleons. The theoretical calculations for these few-body observables are very sensitive to the model used for the nuclear EM current operator, especially its meson-exchange-current (MEC) contributions. Relativistic corrections and possible admixtures of multi-quark states in the nuclear wave function might also be relevant [3]. Additionally, at large momentum transfers,

these EM form factors may offer a unique opportunity to uncover a possible transition in the description of elastic electron scattering off of few-body nuclear systems, from meson-nucleon to quark-gluon degrees of freedom, as predicted by the dimensional-scaling quark model (DSQM) and perturbative QCD (pQCD) [4, 5].

Experimentally, the few-body form factors are determined from elastic electron-nucleus scattering using high intensity beams, high density targets, and large solid angle magnetic spectrometers. There have been extensive experimental investigations of the few-body form factors over the past 50 years at almost every electron accelerator laboratory [6, 7], complemented by equally extensive theoretical calculations and predictions [3, 7, 8]. A recent review can be found in Ref. [9].

This work focuses on a measurement of the ${}^3\text{He}$ EM form factors at Jefferson Lab (JLab). The cross section for elastic scattering of a relativistic electron from the spin $1/2$ ${}^3\text{He}$ nucleus is given, in the one-photon exchange approximation and in natural units, by the formula [10]:

$$\frac{d\sigma}{d\Omega} = \left(\frac{d\sigma}{d\Omega}\right)_{NS} \left[A(Q^2) + B(Q^2) \tan^2\left(\frac{\theta}{2}\right) \right], \quad (1)$$

where

$$\left(\frac{d\sigma}{d\Omega}\right)_{NS} = \frac{(Z\alpha)^2 E' \cos^2\left(\frac{\theta}{2}\right)}{4E^3 \sin^4\left(\frac{\theta}{2}\right)} \quad (2)$$

is the cross section for the scattering of a relativistic electron by a structureless nucleus, and A and B are the elastic structure functions of ${}^3\text{He}$:

$$A(Q^2) = \frac{F_C^2(Q^2) + \mu^2 \tau F_M^2(Q^2)}{1 + \tau}, \quad (3)$$

$$B(Q^2) = 2\tau \mu^2 F_M^2(Q^2), \quad (4)$$

with F_C and F_M being the charge and magnetic form factors of the nucleus. Here, α is the fine-structure constant, Z and μ are the nuclear charge and magnetic moment, E and E' are the incident and scattered electron energies, θ is the electron scattering angle, $Q^2 = 4EE' \sin^2(\theta/2)$ is minus the four-momentum transfer squared, and $\tau = Q^2/4M^2$ with M being the nuclear mass.

The three-body form factors have been theoretically investigated by several groups, using different techniques to solve for the nuclear ground states, and a variety of models for the nuclear EM current [11–14]. The most recent calculation of the ${}^3\text{H}$ and ${}^3\text{He}$ form factors in the Q^2 -range of the experiment is that of Refs. [2, 15]. It uses the pair-correlated hyperspherical harmonics (HH) method [16] to construct high-precision nuclear wave functions and goes beyond the impulse approximation (IA) (where the electron interacts with just one of the nucleon constituents) by including MEC, whose main contributions are constructed to satisfy the current conservation relation with the given Hamiltonian [15]. Part of the present work is the extension of the above method to

evolve the ${}^3\text{He}$ F_C and F_M form factors (see Figures 1-3) to large momentum transfers, using the (uncorrelated) HH expansion to solve for the ${}^3\text{He}$ wave function from the Argonne AV18 nucleon-nucleon (NN) and Urbana UIX three-nucleon ($3N$) interactions [17]. The calculations include MEC contributions arising from π -, ρ - and ω -meson exchanges, as well as the $\rho\pi\gamma$ and $\omega\pi\gamma$ charge transition couplings.

At large Q^2 , elastic scattering from few-body nuclear systems like ${}^3\text{He}$ may be partly due to, or even dominated by, contributions from the electron's interaction with the nucleons' constituent quarks. A purely phenomenological “hybrid quark-hadron” approach includes multi-quark states for overlapping nucleons in the nuclear wave function, which augment the IA approach [18]. The field theory approach of the DSQM, later substantiated within the pQCD framework [5], is based on dimensional scaling of high energy amplitudes using quark counting. This leads to the asymptotic prediction $\sqrt{F_C(Q^2)} \sim (Q^2)^{1-3A}$, where $A = 3$ for the ${}^3\text{He}$ case (see Ref. [4]).

The experiment (E04-018) used the Continuous Electron Beam (100% duty factor) Accelerator and Hall A Facilities of JLab. Electrons scattered from a high density cryogenic ${}^3\text{He}$ target were detected in the Left High Resolution Spectrometer (e-HRS). To suppress backgrounds and unambiguously separate elastic from inelastic processes, recoil helium nuclei were detected in the Right HRS (h-HRS) in coincidence with the scattered electrons. The incident-beam energy ranged between 0.688 and 3.304 GeV. The beam current ranged between 29 and $99\mu\text{A}$. The cryogenic target system contained gaseous ${}^3\text{He}$ and liquid hydrogen cells of length $T=20$ cm. The ${}^3\text{He}$ gas was pressurized to 13.7-14.2 atm at a temperature of 7.1-8.7 K, resulting in a density of 0.057-0.070 g/cm^3 . Two Al foils separated by 20 cm were used to measure any possible contribution to the cross section from the Al end-caps of the target cells.

Scattered electrons were detected in the e-HRS using two planes of scintillators to form an “electron” trigger, a pair of drift chambers for electron track reconstruction, and a gas threshold Čerenkov counter and a lead-glass calorimeter for electron identification. Recoil helium nuclei were detected in the h-HRS using two planes of scintillators to form a “recoil” trigger and a pair of drift chambers for recoil track reconstruction. The event trigger consisted of a coincidence between the two HRS triggers. Details on the Hall A Facility and all associated instrumentation used are given in Refs. [19, 20].

Particles in the e-HRS were identified as electrons on the basis of a minimal pulse height in the Čerenkov counter and the energy deposited in the calorimeter, consistent with the momentum as determined from the drift chamber track using the spectrometer's optical properties. Particles in the h-HRS were identified as ${}^3\text{He}$ nuclei on the basis of their energy deposition in the first scintillator plane. Electron- ${}^3\text{He}$ (e - ${}^3\text{He}$) coincidence events, consistent with elastic kinematics, were identified using the relative time-of-flight (TOF) between the electron

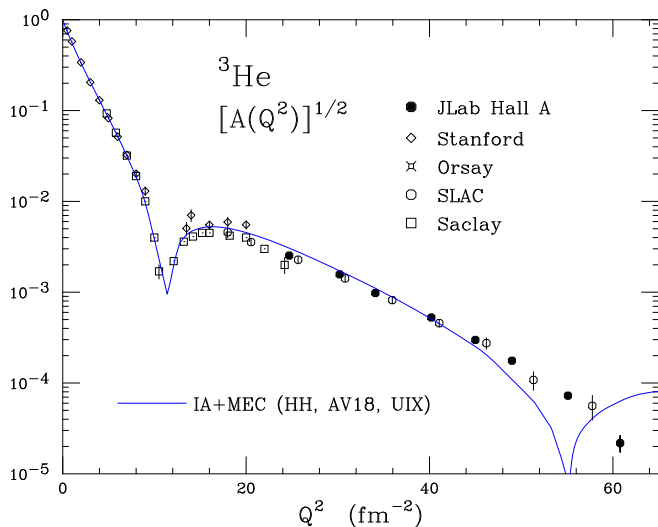


FIG. 1: ^3He elastic structure function $A(Q^2)$ data from this experiment, compared to selected previous data and the present theoretical calculation with the hyperspherical harmonics variational method (see text).

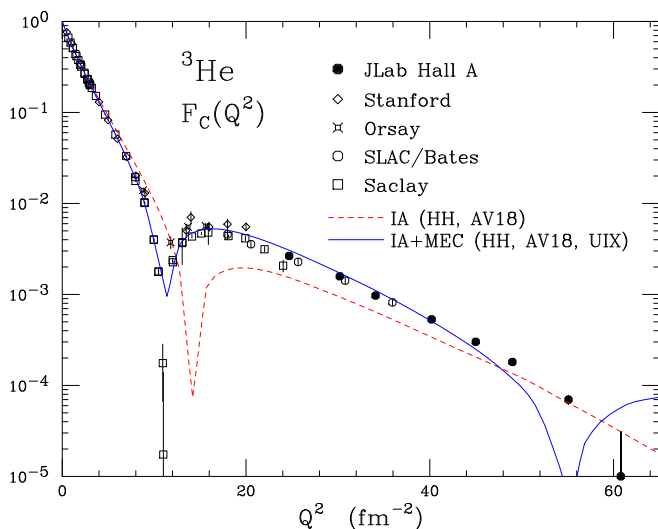


FIG. 2: ^3He charge form factor $F_C(Q^2)$ data from this experiment, compared to selected previous data and the present theoretical calculation with the hyperspherical harmonics variational method (see text).

and recoil triggers after imposing the above particle identification “cuts”. To check the overall normalization, elastic e -proton (e - p) scattering was measured at several kinematics. The e - p data are in excellent agreement with the world data, as described in Ref. [19].

The elastic e - ^3He cross section values were calculated using the formula:

$$\left[\frac{d\sigma}{d\Omega}(E, \theta) \right]_{exp} = \frac{N_{er} C_{cor}}{N_b N_t (\Delta\Omega)_{MC} F(Q^2, T)}, \quad (5)$$

where N_{er} is the number of electron-recoil ^3He elastic events, N_b is the number of incident beam electrons, N_t

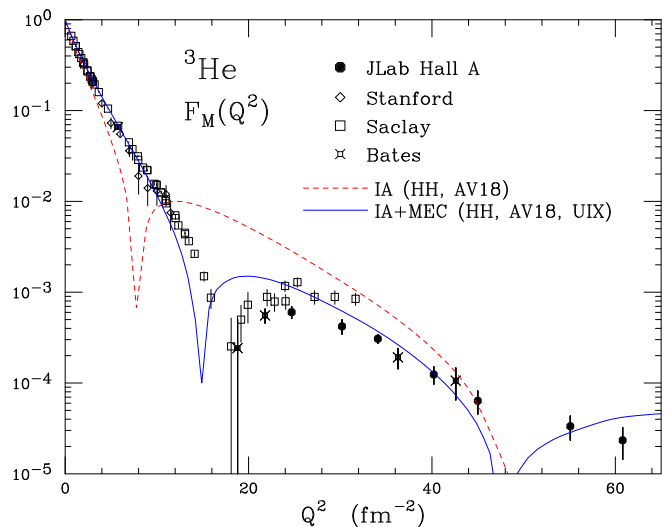


FIG. 3: ^3He magnetic form factor $F_M(Q^2)$ data from this experiment, compared to selected previous data and the present theoretical calculation with the hyperspherical harmonics variational method (see text).

is the number of target nuclei/cm², $(\Delta\Omega)_{MC}$ is the effective coincidence solid angle (which includes most radiative effects) from a Monte Carlo simulation, F is the portion of the radiative corrections that depends only on Q^2 and T (1.07-1.10) [21], and $C_{cor} = C_{det} C_{cdt} C_{rni} C_{den}$. Here, C_{det} is the correction for the inefficiency of the Čerenkov counter and the calorimeter (1.01) (the scintillator counter hodoscopes were found to be essentially 100% efficient), C_{cdt} is the computer dead-time correction (1.04-1.56), C_{rni} is a correction for losses of recoil nuclei due to nuclear interactions in the target cell and vacuum windows (1.02-1.08), and C_{den} is a correction to the target density due to beam heating effects (ranging between 1.02 at 29 μA and 1.07 at 99 μA). There were no contributions to the elastic e - ^3He cross section from events originating in the target cell end-caps, as determined from runs with the empty replica target. The e - p elastic cross section values were determined similarly.

The effective coincidence solid angle was evaluated with a Monte Carlo computer code that simulated elastic electron-nucleus scattering under identical conditions as our measurements [21]. The code tracked scattered electrons and recoil nuclei from the target to the detectors through the two HRS systems using optical models based on magnetic field measurements and precision position surveys of their elements. The effects from ionization energy losses and multiple scattering in the target and vacuum windows were taken into account for both electrons and recoil nuclei. Bremsstrahlung radiation losses for both incident and scattered electrons in the target and vacuum windows, as well as internal radiative effects, were also taken into account. It should be noted that the two-photon exchange effect is not included in the radiative corrections implementation. A credible correction to the data for this effect should be

E GeV	θ deg.	Q^2 fm^{-2}	$d\sigma/d\Omega$ cm^2/sr
3.304	17.52	24.7	$(2.29 \pm 0.12) \times 10^{-35}$
0.7391	97.78	24.7	$(2.80 \pm 0.20) \times 10^{-37}$
3.304	19.50	30.2	$(5.16 \pm 0.29) \times 10^{-36}$
0.7391	118.99	30.2	$(3.95 \pm 0.38) \times 10^{-38}$
0.6876	139.99	30.2	$(1.51 \pm 0.19) \times 10^{-38}$
3.304	20.83	34.1	$(1.57 \pm 0.10) \times 10^{-36}$
0.8157	113.01	34.1	$(1.43 \pm 0.13) \times 10^{-38}$
0.7394	139.91	34.1	$(6.41 \pm 0.59) \times 10^{-39}$
3.304	22.82	40.2	$(3.03 \pm 0.21) \times 10^{-37}$
0.8177	139.53	40.2	$(1.24 \pm 0.16) \times 10^{-39}$
3.304	24.28	45.0	$(7.56 \pm 0.75) \times 10^{-38}$
0.9330	119.94	45.0	$(6.84 \pm 1.10) \times 10^{-40}$
0.8726	140.66	45.0	$(3.24 \pm 0.51) \times 10^{-40}$
3.304	25.47	49.0	$(2.13 \pm 0.35) \times 10^{-38}$
3.304	27.24	55.1	$(2.77 \pm 0.39) \times 10^{-39}$
0.9893	140.31	55.1	$(3.27 \pm 0.13) \times 10^{-41}$
3.304	28.86	60.8	$(2.14 \pm 0.72) \times 10^{-40}$
1.052	140.51	60.8	$(1.13 \pm 0.80) \times 10^{-41}$

TABLE I: Values of beam energy, scattering angle, effective Q^2 , and elastic e - ${}^3\text{He}$ cross section with total error (statistical and systematic added in quadrature).

Q^2 fm^{-2}	$ F_C $	$ F_M $
24.7	$(2.65 \pm 0.06) \times 10^{-3}$	$(6.03 \pm 0.91) \times 10^{-4}$
30.2	$(1.58 \pm 0.05) \times 10^{-3}$	$(4.21 \pm 0.75) \times 10^{-4}$
34.1	$(9.73 \pm 0.34) \times 10^{-4}$	$(3.07 \pm 0.35) \times 10^{-4}$
40.2	$(5.32 \pm 0.21) \times 10^{-4}$	$(1.24 \pm 0.27) \times 10^{-4}$
45.0	$(3.02 \pm 0.16) \times 10^{-4}$	$(6.37 \pm 1.83) \times 10^{-5}$
49.0	$(1.81 \pm 0.15) \times 10^{-4}$	—
55.1	$(6.97 \pm 0.72) \times 10^{-5}$	$(3.34 \pm 1.00) \times 10^{-5}$
60.8	$(1.00 \pm 2.10) \times 10^{-5}$	$(2.34 \pm 0.90) \times 10^{-5}$

TABLE II: Effective Q^2 , and ${}^3\text{He}$ charge and magnetic form factors (absolute values) with total errors (statistical and systematic added in quadrature).

based on established complementary calculations, which are not yet fully available for the entire kinematic range of our measurements. A correction (not only for this, but for all available ${}^3\text{He}$ elastic data sets) will have to wait for the completion and further understanding of ongoing calculations [22].

The Rosenbluth cross section formula (1) is based on the assumption that the wave functions of the incident and scattered electrons are described by plane waves. In reality, the charge of the nucleus distorts these wave functions, necessitating a correction to the formula [1]. This Coulomb effect shifts the Q^2 value of the interaction to an “effective” value, given by $Q^2_{eff} = (1 + 3Z\alpha\hbar c/2R_{eq}E)^2 Q^2$, where R_{eq} is the hard sphere equivalent radius of the nucleus, \hbar is the Planck constant and c is the speed of light. This correction allows for a form factor extraction using a Rosenbluth separation of cross section values determined, at each kinematic point, at the same Q^2_{eff} [24]. This approach was followed in this experiment and the results are given in terms of the effective Q^2 in Tables I and II and plotted in Figs 1-3.

At each kinematic point, the “reduced” cross section, $(d\sigma/d\Omega)_r$, defined using equations (1-4) and the experimentally determined cross section $[d\sigma/d\Omega]_{exp}$

$$\left(\frac{d\sigma}{d\Omega}\right)_r = \left(\frac{d\sigma}{d\Omega}\right)_{exp} \left(\frac{d\sigma}{d\Omega}\right)_{NS}^{-1} (1 + \tau) = \left(F_C^2 + \mu^2 \frac{\tau}{\epsilon} F_M^2\right) \quad (6)$$

was plotted, at same values of Q^2_{eff} , versus $\mu^2 \tau / \epsilon$ (Rosenbluth plot), and the ${}^3\text{He}$ F_C^2 and F_M^2 values were extracted by a linear fit. Here, $\epsilon = [1 + 2(1 + \tau) \tan^2(\theta/2)]^{-1}$ is the degree of the longitudinal polarization of the exchanged virtual photon. It should be noted that at $Q^2 = 49 \text{ fm}^{-2}$ data were taken only at a forward angle (25.47°) and that the F_C value was extracted under the reasonable assumption that the F_M does not contribute to the cross section.

The $A(Q^2)$ values from this experiment are shown in Fig. 1 along with previous data from a SLAC experiment [23], which performed elastic scattering at a fixed angle $\theta = 8^\circ$, and selected data from other laboratories [24–26]. It is evident that the JLab and SLAC data sets are in excellent agreement. Also shown is the present IA+MEC theoretical calculation (see below). The (absolute) values of the ${}^3\text{He}$ F_C and F_M from this work are shown in Figs. 2 and 3 along with previous Stanford [24], Orsay [25], SLAC [23], Saclay [26] and MIT/Bates [27] data. Not shown, for clarity, are the low Q^2 MIT/Bates data [28]. In all three figures, the error bars represent statistical and systematic uncertainties added in quadrature. The new F_C data are in excellent agreement with data extracted from a Rosenbluth separation between SLAC forward angle ($\theta = 8^\circ$) cross sections and interpolations of backward angle (160°) MIT/Bates [27] cross sections, labeled as “SLAC/Bates” data in Fig. 2. The new F_M data are in excellent agreement with the MIT/Bates data taken at $\theta = 160^\circ$, but in very strong disagreement with the Saclay data taken at $\theta = 155^\circ$. The F_M datum at $Q^2 = 24.7 \text{ fm}^{-2}$ has been extracted from a Rosenbluth separation of a forward- and a medium- θ JLab-measured cross section and an interpolated cross section from the $\theta = 160^\circ$ MIT/Bates data set [27].

An updated extension of the latest theoretical calculation based on the IA with inclusion of MEC, which used the HH variational method to calculate the ${}^3\text{He}$ wave function, as described above and outlined in Ref. [15], was performed for this work and is shown in Figs. 2 and 3. The calculation is, in general, in qualitative agreement with the data even at large momentum transfers where theoretical uncertainties may become sizable. Of note is the long-standing disagreement between the calculation and the data in the Q^2 range around the first diffraction minimum of the ${}^3\text{He}$ F_M . It is not presently clear if this is due to a missing piece of important physics in the non-relativistic theory or to the need for a fully relativistic calculation. The presently available relativistic calculation based on the Gross equation [29] will be able to be compared to the new data when the not-yet-calculated

$\rho\pi\gamma$ interaction current is included in this so called “relativistic impulse approximation” approach [9].

It should be noted that all seminal, older calculations of the ${}^3\text{He}$ form factors (not shown in Figs. 2 and 3) based on the Faddeev formalism [11, 12] or the Monte Carlo variational method [13, 14], are in qualitative agreement with the data in predicting a diffractive structure for both form factors, and also indicative, in general, of large MEC contributions. Also, it is evident that the diffractive pattern of the JLab data is incompatible with the asymptotic-falloff DSQM prediction [4], and that it supports the conclusion of Ref. [30] that the onset of asymptotic scaling must be at a Q^2 value much greater than 100 fm^{-2} , not presently accessible at JLab for ${}^3\text{He}$.

In summary, we have measured the ${}^3\text{He}$ charge and magnetic form factors in the range $25\text{ fm}^{-2} \leq Q^2 \leq 61\text{ fm}^{-2}$. The results are in qualitative agreement with theoretical calculations based on the IA with inclusion of MEC. The new data strongly indicate the presence of an apparent second diffraction minimum for the magnetic form factor in the vicinity of $Q^2 = 50\text{ fm}^{-2}$ as well as the possible presence of a second diffraction minimum for the

charge form factor located at a Q^2 value just beyond 60 fm^{-2} . The results will constrain inherent uncertainties of the theoretical calculations and lead, together with previous large Q^2 data on the deuteron [31], tritium [26] and ${}^4\text{He}$ [19] EM form factors, to the development of a consistent hadronic model describing the internal EM structure and dynamics of few-body nuclear systems.

We acknowledge the outstanding support of the staff of the Accelerator and Physics Divisions of JLab that made this experiment possible. We are grateful to Drs. D. Riska, R. Schiavilla, and R. Wiringa for kindly providing their theoretically motivating calculations for the proposal of this experiment, and to Drs. F. Gross, R. Schiavilla, and W. Melnitchouk for valuable discussions and support. This material is based upon work supported by the U.S. Department of Energy (DOE), Office of Science, Office of Nuclear Physics under contract DE-AC05-06OR23177. This work was also supported by DOE awards DE-AC02-06CH11357 and DE-FG02-96ER40950, National Science Foundation awards NSF-PHY-0701679, NSF-PHY-1405814 and NSF-PHY-0652713, the Kent State University Council, and the INFN.

-
- [1] Herbert Uberall, *Electron Scattering from Complex Nuclei*, Academic Press (1971).
- [2] L. E. Marcucci, D. O. Riska, and R. Schiavilla, Phys. Rev. **C58**, 3069 (1998).
- [3] J. Carlson and R. Schiavilla, Rev. Mod. Phys. **70**, 743 (1998); and references therein.
- [4] S. J. Brodsky and B. T. Chertok, Phys. Rev. **D14**, 3003 (1976); B. T. Chertok, Phys. Rev. Lett. **41**, 1155 (1978).
- [5] S. J. Brodsky and C.-R. Ji, Comments Nucl. Part. Phys. **13**, 213 (1984); and references therein.
- [6] I. Sick, Prog. Part. Nucl. Phys. **47**, 245 (2001).
- [7] R. Gilman and F. Gross, J. Phys. **G28**, R37 (2002).
- [8] R. J. Holt and R. Gilman, Rept. Prog. Phys. **75**, 086301 (2012).
- [9] L. E. Marcucci, F. Gross, M. T. Peña, M. Piarulli, R. Schiavilla, I. Sick, A. Stadler, J. W. Van Orden, and M. Viviani, J. Phys. **G43**, 023002 (2016).
- [10] E. Hadjimichael, *International Review of Nuclear Physics*, Vol. 3, World Scientific, Singapore (1985).
- [11] E. Hadjimichael, B. Goulard, and R. Bornais, Phys. Rev. **C27**, 831 (1983); E. Hadjimichael, Phys. Lett. **B172**, 156 (1986).
- [12] W. Strueve, Ch. Hadjuk, P. U. Sauer, and W. Theis, Nucl. Phys. **A465**, 651 (1987).
- [13] R. Schiavilla, V. R. Pandharipande, and D. O. Riska, Phys. Rev. **C40**, 2294 (1989); R. Schiavilla, V. R. Pandharipande, and D. O. Riska, Phys. Rev. **C41**, 309 (1990).
- [14] R. B. Wiringa, Phys. Rev. **C43**, 1585 (1991).
- [15] L. E. Marcucci, M. Viviani, R. Schiavilla, A. Kievsky, and S. Rosati, Phys. Rev. **C72**, 014001 (2005).
- [16] A. Kievsky, S. Rosati, M. Viviani, L. E. Marcucci, and L. Girlanda, J. Phys. **G35**, 063101 (2008); and references therein.
- [17] R. B. Wiringa, V. G. J. Stoks, and R. Schiavilla, Phys. Rev. **C51**, 38 (1995); B. S. Pudliner, V. R. Pandharipande, J. Carlson, S. C. Pieper, and R. B. Wiringa, Phys. Rev. **C56**, 1720 (1997).
- [18] H. Dijk and B. L. G. Bakker, Nucl. Phys. **A531**, 555 (1991); and references therein.
- [19] A. Camsonne *et al.*, Phys. Rev. Lett. **112**, 132503 (2014).
- [20] J. Alcorn *et al.*, Nucl. Instrum. Methods **A522**, 294 (2004).
- [21] A. T. Katramatou, Kent State University preprint KSU-CNR-14-11, December 2011.
- [22] P. G. Blunden, W. Melnitchuk, and J. A. Tjon, Phys. Rev. **66**, 018202 (2010); A. P. Kobushkin and Yu. V. Timoshenko, Phys. Rev. **C88**, 044002 (2013); A. P. Kobushkin and W. Melnitchouk, private communications.
- [23] R. G. Arnold, B. T. Chertok, S. Rock, W. P. Schütz, Z. M. Szalata, D. Day, J. S. McCarthy, F. Martin, B. A. Mecking, I. Sick, and G. Tamas, Phys. Rev. Lett. **40**, 1429 (1978).
- [24] J. S. McCarthy, I. Sick, and R. R. Whitney, Phys. Rev. **C15**, 1396 (1977); and references therein.
- [25] M. Bernheim, D. Blum, W. McGill, R. Riskalla, C. Trail, T. Stovall, and D. Vinciguerra, Lett. Nuovo Cimento **5**, 431 (1972).
- [26] A. Amroun *et al.*, Nucl. Phys. **A579**, 596 (1994); and references therein.
- [27] I. Nakagawa *et al.*, Phys. Rev. Lett. **86**, 5446 (2001).
- [28] P. C. Dunn *et al.*, Phys. Rev. **C27**, 71 (1983); D. H. Beck *et al.*, Phys. Rev. **C30**, 1403 (1984).
- [29] S. A. Pinto, A. Stadler, and F. Gross, Phys. Rev. **C79**, 054006 (2010); Phys. Rev. **C81**, 014007 (2011).
- [30] R. J. Holt, Phys. Rev. **C41**, 2400 (1990).
- [31] L. C. Alexa *et al.*, Phys. Rev. Lett. **82** 1374 (1999); P. E. Bosted *et al.*, Phys. Rev. **C42**, 38 (1990).